Computer Physics Communications 252 (2020) 107130

Contents lists available at ScienceDirect

Computer Physics Communications

journal homepage: www.elsevier.com/locate/cpc

CALANIE: Anisotropic elastic correction to the total energy, to mitigate the effect of periodic boundary conditions☆,☆☆

Pui-Wai Ma *, S.L. Dudarev

Culham Centre for Fusion Energy, UK Atomic Energy Authority, Culham Science Centre, Abingdon, Oxfordshire, OX14 3DB, United Kingdom

ARTICLE INFO

Article history:
Received 15 July 2019
Received in revised form 27 November 2019
Accepted 7 December 2019
Available online 26 December 2019

Keywords:
Point defects
Elastic dipole tensor
Anisotropic elasticity
Periodic boundary conditions
Ab initio calculations

ABSTRACT

CALANIE (CALculation of ANIsotropic Elastic energy) computer program evaluates the elastic interaction correction to the total energy of a localized object, for example a defect in a material simulated using an *ab initio* or molecular statics approach, resulting from the use of periodic boundary conditions. The correction, computed using a fully elastically anisotropic Green's function formalism, arises from the elastic interaction between a defect and its own periodically translated images. The long-range field of elastic displacements produced by the defect is described in the elastic dipole approximation. Applications of the method are illustrated by two case studies, one involving an *ab initio* investigation of point defects and vacancy migration in FCC gold, and another a molecular statics simulation of a dislocation loop. We explore the convergence of the method as a function of the simulation cell size, and note the significance of taking into account the elastic correction in the limit where the size of the defect is comparable with the size of the simulation cell.

Program summary

Program Title: CALANIE, version 2.0
Program Files doi: http://dx.doi.org/10.17632/3h6xffk9h6.1
Licensing provisions: Apache License, Version 2.0
Programming language: C/C++
Nature of problem: Periodic boundary conditions (PBCs) are often used in the context of *ab initio* and molecular statics atomic scale simulations. A localized defect in a crystalline material, simulated using PBCs, interacts elastically with its own periodically translated images, and this gives rise to a systematic error in the computed defect formation and migration energies. Evaluating the correction to the total energy resulting from effects of elastic interaction between a defect and its periodic images, to alleviate the contribution to the total energy arising from PBCs, is an essential aspect of any accurate total energy calculation performed using PBCs.
Solution method: The energy of interaction between a localized defect and its periodically translated images is computed in the linear elasticity approximation. The energy of elastic interaction is expressed analytically in terms of the elastic dipole tensor of the defect and elastic Green's function. Elements of the dipole tensor are computed as a part of the simulation evaluating the formation energy of the defect. Elastic Green's function and its first and second derivatives are computed numerically from the elastic constants of the material. The method and the corresponding numerical procedures are implemented in the CALANIE computer program. The program evaluates matrix elements of the elastic dipole tensor of a localized defect and the elastic correction to the total energy arising from the use of periodic boundary conditions.
Restrictions: The approach assumes the validity of the linear elasticity approximation. This limits the accuracy of evaluation of the elastic correction, which becomes less precise if the size of the defect is comparable with the size of the simulation cell.
Unusual features: An open source code, containing full detail of the relevant theoretical concepts, algorithms and numerical implementation.

☆ This paper and its associated computer program are available via the Computer Physics Communication homepage on ScienceDirect (http://www.sciencedirect.com/science/journal/00104655).

☆☆ The review of this paper was arranged by Prof. D.P. Landau.

* Corresponding author.
E-mail addresses: leo.ma@ukaea.uk (P.-W. Ma), sergei.dudarev@ukaea.uk (S.L. Dudarev).

https://doi.org/10.1016/j.cpc.2019.107130
0010-4655/

1. Introduction

Mechanical deformation, or irradiation by energetic particles, produces a variety of defects in a crystalline material, for example dislocation loops, vacancy clusters, voids, Frenkel pairs, and extended dislocations [1–4]. Defect structures evolve under the effect of external stress and temperature. Defects migrate, segregate and agglomerate as a result of elastic interaction, mediated by the deformation of the crystal lattice [5–9]. Evolution of defect structures changes mechanical and physical properties of the material [10].

Electronic and atomic scale simulations are the indispensable numerical simulation tools that help understand the fundamental laws driving microstructure evolution and its effect on mechanical and physical properties of the materials. *Ab initio* density function theory (DFT) calculations [11,12] are commonly used for computing the formation and migration energies of small defects. The energy of formation of a defect at equilibrium determines the relative probability of its occurrence, whereas the energy of migration determines the rate of thermal transformation of an already formed defect structure. Molecular dynamics [2,3] and kinetic Monte Carlo [13–15] simulations provide information about reaction rates and relaxation pathways characterizing complex configurations of defects.

To avoid considering surface effects, simulations are often performed using periodic boundary conditions (PBCs). Through periodic boundary conditions, a spatially localized defect situated in a simulation cell interacts elastically with an infinite number of its own images situated in periodically translated simulation cells [6–9]. Since elastic fields effectively have infinite range, and the energy E_{el} of elastic interaction between any two defects varies as the inverse cube of distance R between the defects $E_{el} \sim R^{-3}$ [8], if a relatively small cell is used in a simulation, the elastic energy of interaction between a defect and its periodic images can be substantial. This can affect the accuracy of calculations performed using PBCs and make the total energy data strongly dependent on the cell size. Although in principle the issue can be partially circumvented using a larger simulation cell, in practice this may not necessarily be a realistic option because of the limitations imposed by the available computational resources or numerical algorithms. For example, in a conventional DFT calculation, the simulation cell size is still limited to a few hundred atoms.

A possible way forward is to introduce an elastic correction to the calculated formation energy. A first order correction, assuming the linear elasticity approximation, can be derived using the elastic dipole tensor formalism [6–9], which only requires knowing the elements P_{ij} of elastic dipole tensor of the defect and the elastic constants tensor C_{ijkl} of the material. This information can be readily derived from the same DFT or molecular statics calculation.

An elastic dipole tensor fully defines the elastic field produced by a defect in a material [8,16,17]. The elastic strain field associated with a localized defect, or even a large but still localized agglomerate of defects, can be expressed in an explicit analytical form using the notion of the dipole tensor. From the dipole tensor it is also possible to evaluate the relaxation volume tensor of a defect or an ensemble of defects [17,18]. By considering all the defects in a certain volume element of the material as a compound object characterized by its dipole tensor, it is possible to formulate a continuum model spanning the spatial scale many orders of magnitude larger than an atomistic simulation [17]. In addition, the notion of the dipole tensor enables treating interactions between defects. A dipole tensor can be defined for an arbitrarily large configuration of defects, for example the entire defect structure created in a collision cascade simulation can be described by a dipole tensor, enabling extending the treatment to a macroscopic scale [17,18].

In previous studies, we derived analytical equations for treating the elastic fields of defects in a simulation cell using periodic boundary conditions [8]. We have also derived equations for evaluating the elastic correction to the energy of a localized defect [9], and implemented them in our program CALANIE. It is appropriate to make this code, suitable for evaluating the elastic correction to the total energy, and for calculating the elastic dipole tensor of a defect in a simulation cell, available as an open source computer program. Full numerical and algorithmic aspects of the code are described below.

In what follows we review the fundamental theory and explain the meaning of various equations. We also discuss the numerical implementation of the method, followed by the details of the compilation procedure, and the format of input and output files. We give two examples illustrating applications of the code. The first example involves *ab initio* calculations of point defects and vacancy migration in FCC gold. This example illustrates the applicability of CALANIE to both equilibrium and non-equilibrium configurations. The second example illustrates molecular statics calculations of mesoscopic size dislocation loops. We investigate the numerical convergence of elements of the dipole tensor and formation energy of a defect as a function of the simulation box size, and the significance of applying elastic correction to the formation energy in the limit where the simulation cell is relatively small.

2. Theory

2.1. Elastic dipole tensor

In a continuum elasticity theory, the elastic strain energy of a defect in an infinite medium is defined as a volume integral over the entire space:

$$E_D = \frac{1}{2}\int_V \sigma_{ij}(\mathbf{r})\epsilon_{ij}(\mathbf{r})dV, \tag{1}$$

where ϵ_{ij} and σ_{ij} are the coordinate-dependent elastic strain and stress fields. Assuming the validity of the linear elasticity approximation, we write $\sigma_{ij} = C_{ijkl}\epsilon_{kl}$, where C_{ijkl} is the rank four elastic constant tensor. The above equation now acquires the form

$$E_D = \frac{1}{2}\int_V C_{ijkl}\epsilon_{kl}(\mathbf{r})\epsilon_{ij}(\mathbf{r})dV. \tag{2}$$

In the presence of infinitesimal external strain ϵ_{ij}^{ext}, elastic energy E_D can be represented by a Taylor series expansion:

$$E_D(\epsilon_{ij}^{ext}) = E_D(\epsilon_{ij}^{ext}=0) + \left(\frac{\delta E_D}{\delta \epsilon_{ij}^{ext}}\right)_{\epsilon_{ij}^{ext}=0} \epsilon_{ij}^{ext} + \cdots. \tag{3}$$

The energy of elastic interaction between a defect and external strain field is defined as [16]:

$$E = -P_{ij}\epsilon_{ij}^{ext}, \tag{4}$$

where P_{ij} is the elastic dipole tensor of a defect. Comparing Eqs. (3) and (4), we can identify the dipole tensor with a volume integral

$$P_{ij} = -\left(\frac{\delta E_D}{\delta \epsilon_{ij}^{ext}}\right)_{\epsilon_{ij}^{ext}=0} = -\int_V \sigma_{ij}^{D} dV, \tag{5}$$

where σ_{ij}^{D} is the stress field resulting from the presence of a defect in the medium.

In practice, calculations are not performed in an infinite medium. Infinite medium is simulated by applying periodic

boundary conditions to a finite size simulation cell. This is equivalent to placing N identical defects in an infinite medium in the form of a lattice of defects, defined by the translation vectors of the simulation cell, and taking the limit $N \to \infty$.

We can write the total stress as a linear sum of contributions from all the identical periodically translated defects as [8],

$$\int_V \sigma_{ij}^D dV + \sum_{n\neq 0} \int_V \sigma_{ij}^{Im,n} dV = N \int_V \sigma_{ij}^D dV, \tag{6}$$

where $\sigma_{ij}^{Im,n}$ is the stress field due to the nth image of the defect. Dividing both sides of the above equation by N, we find

$$\int_V \sigma_{ij}^D dV = \frac{1}{N} \int_V \left(\sigma_{ij}^D + \sum_{n\neq 0} \sigma_{ij}^{Im,n} \right) dV = \int_{V_{cell}} \sigma_{ij} dV. \tag{7}$$

Therefore, the total stress induced by a defect, integrated over infinite medium, equals the total stress of the defect plus all its images, integrated over the simulation cell in a periodic boundary condition calculation. The proof is based on the linear elasticity approximation stating that the total stress field is a linear sum of stresses produced by the defect and all its images, and on the fact that the stress field in a simulation cell is the same as in any periodically translated cell. The simulation box used for a defect calculation needs to be of exactly the same shape and size as in the corresponding perfect lattice case, to mimic the infinite medium conditions.

Eq. (5) can now be written in terms of the macrostress $\bar{\sigma}_{ij}$ developing in a simulation cell under the PBCs, namely

$$P_{ij} = -\int_{V_{cell}} \sigma_{ij} dV = -V_{cell} \bar{\sigma}_{ij}. \tag{8}$$

The macrostress $\bar{\sigma}_{ij}$ is identical to the average stress in the cell. We note that the volume integral may be ill-defined if the equation is applied to a discrete atomistic configuration. Nevertheless, the expression remains valid and can be derived in the discrete atomistic limit [18].

Provided that the total energy of the system depends only on atomic positions, such that $E_D = E_D(\{\mathbf{R}_n\})$, where $\{\mathbf{R}_n\}$ is a set of coordinates, we write

$$P_{ij} = -\left(\frac{\delta E_D}{\delta \epsilon_{ij}^{ext}} \right)_{\epsilon_{ij}^{ext}=0} = -\sum_{n,\alpha} \frac{\delta E_D}{\delta R_{n,\alpha}} \left(\frac{\delta R_{n,\alpha}}{\delta \epsilon_{ij}^{ext}} \right)_{\epsilon_{ij}^{ext}=0}. \tag{9}$$

Here n is the index of an atom and α refers to a Cartesian coordinate. The first term in the right-hand side is the component of force $F_{n,\alpha}$ acting on an atom. The second term can be obtained assuming that all the position vectors move in response to the applied external strain according to the transformation

$$\mathbf{R} \to (\mathbf{I} + \boldsymbol{\epsilon})\mathbf{R}, \tag{10}$$

which leads to

$$\left(\frac{\delta R_{n,\alpha}}{\delta \epsilon_{ij}^{ext}} \right)_{\epsilon_{ij}^{ext}=0} = R_{n,j} \delta_{\alpha i}. \tag{11}$$

The dipole tensor then becomes

$$P_{ij} = \sum_n F_{n,i} R_{n,j} = -V_{cell} \bar{\sigma}_{ij}. \tag{12}$$

This is the same formula for evaluating the dipole tensor as that derived using the Kanzaki force method [16]. In agreement with the Virial Theorem at 0 K, the right-hand side of the above equation can also be expressed in terms of the macrostress, i.e. the global stress arising in a simulation cell due to the presence of a defect in it.

In a DFT calculation, the macrostress developing in a cell due to the presence of a defect in it, is calculated from the variation of the total energy treated as a function of strain, taken in full tensorial form. In both the continuum and discrete limits, we arrive at exactly the same expression for the dipole tensor. This equation relates linear elasticity to both electronic and atomic scale simulations.

If the cell used for simulating a defect structure has a different shape in comparison with the perfect lattice case, the way of treating the problem is to assume as if the simulation cell is subjected to external strain. The strain tensor describing the external applied strain $\boldsymbol{\epsilon}^{app}$, given that $\|\epsilon^{app}\| \ll 1$, relates the perfect and deformed simulation cells as follows

$$\mathbf{V}^{perf}(\mathbf{I} + \boldsymbol{\epsilon}^{app}) = \mathbf{V}^{def}, \tag{13}$$

where $\mathbf{I}$ is the identity matrix, $\mathbf{V}^{perf} = \{\mathbf{L}_1^{perf}, \mathbf{L}_2^{perf}, \mathbf{L}_3^{perf}\}$ is the matrix of translation vectors of the perfect lattice cell and $\mathbf{V}^{def} = \{\mathbf{L}_1^{def}, \mathbf{L}_2^{def}, \mathbf{L}_3^{def}\}$ is the matrix of translation vectors of the cell containing a defect. Therefore the strain tensor is simply

$$\boldsymbol{\epsilon}^{app} = (\mathbf{V}^{perf})^{-1} \mathbf{V}^{def} - \mathbf{I}. \tag{14}$$

Whenever an applied strain is present, the dipole tensor should be evaluated using the expression [6,7,9]

$$P_{ij} = V_{cell}(C_{ijkl} \epsilon_{kl}^{app} - \bar{\sigma}_{ij}). \tag{15}$$

There are other methods, using which one can deduce the elastic dipole tensor from an atomic scale simulation [6,16,19]. Varvenne and Clouet [7] concluded that only the residual stress method described above is tractable and practical in the limit of a small simulation cell, especially in relation to *ab initio* calculations. Below we explore the convergence of P_{ij}, and assess the effect of the simulation cell size on the elastic correction energy.

For a linear defect, such as a self-interstitial atom (SIA) crowdion defect, we write [8]:

$$P_{ij} = C_{ijkl} \left(\Omega^{(1)} n_k n_l + \frac{\Omega^{(2)}}{3} \delta_{kl} \right) \tag{16}$$

where $\mathbf{n} = (\cos\phi \sin\theta, \sin\phi \sin\theta, \cos\theta)$ is a unit vector characterizing the orientation of the axis of the defect, and $\Omega^{(1)}$ and $\Omega^{(2)}$ represent the relative contribution of the anisotropic and isotropic components to the relaxation volume of a defect, where the total relaxation volume of the defect is given by the sum

$$\Omega_{rel} = \Omega^{(1)} + \Omega^{(2)}. \tag{17}$$

Values of $\Omega^{(1)}$ and $\Omega^{(2)}$ can be derived from *ab initio* calculations. This formula can be used for estimating the magnitude of change in the elastic correction energy for a defect that undergoes free rotation [8].

2.2. Elastic correction energy

The formation energy of a defect equals [9]:

$$E_{def}^F = [E_{def}(N_{def}) - E^{app}] - \frac{N_{def}}{N_{perf}} E_{perf}(N_{perf}) - E_{el}^{corr}, \tag{18}$$

where E_{def} is the energy of a simulation cell containing a defect, E_{perf} is the energy of a perfect lattice cell used as a reference configuration, N_{def} is the number of atoms in the cell containing a defect, N_{perf} is the number of atoms in a perfect lattice cell, E^{app} is the contribution to the elastic energy due to the applied strain, and E_{el}^{corr} is the elastic correction energy arising from the PBCs. The energy associated with the external applied strain equals [6]:

$$E^{app} = \frac{V^{perf}}{2} C_{ijkl} \epsilon_{ij}^{app} \epsilon_{kl}^{app} - P_{ij} \epsilon_{ij}^{app}, \tag{19}$$

where V^{ref} is the volume of the simulation cell. We neglect the change of the volume of the cell due to elastic deformation, assuming that the applied strain is small. Taking into account the volume change, proportional to the integral of the trace of elastic strain tensor over the volume of the cell, would imply going beyond the linear elasticity approximation.

The first term in Eq. (19) accounts for the elastic energy associated with the homogeneous deformation of the simulation cell. The second term is the energy of interaction between the defect and external applied strain.

The elastic correction energy E_{el}^{corr} is a part of the total resulting from the use of periodic boundary conditions. It consists of two parts

$$E_{el}^{corr} = E_{DD} + E_{strain}^{corr}. \tag{20}$$

E_{DD} is the energy due to elastic interaction between the defect and its periodic images, described in the elastic dipole–dipole interaction approximation. E_{strain}^{corr} is the self-strain correction energy. Adopting the far-field elasticity approximation, the regularized elastic interaction energy E_{DD} can be written in terms of the elastic dipole tensor and anisotropic elastic Green's function [6–8,20] as

$$E_{DD} = E_{DD}^{total} + E_{DD}^{corr}. \tag{21}$$

The first term

$$E_{DD}^{total} = \frac{1}{2}\sum_{n\neq 0} P_{ij}P_{kl}\frac{\partial}{\partial x_j}\frac{\partial}{\partial x_l}G_{ik}(\mathbf{R}_n) \tag{22}$$

is a sum of pairwise elastic dipole interactions between a defect at the original cell and its periodic images, situated at points $\mathbf{R}_n$. This sum is conditionally convergent, see Refs. [6,8]. The second term

$$E_{DD}^{corr} = -\frac{1}{2V_{cell}}\sum_{n\neq 0}\int_{V_{cell}} P_{ij}P_{kl}\frac{\partial}{\partial x_j}\frac{\partial}{\partial x_l}G_{ik}(\mathbf{R}_n - \mathbf{r})d^3r \tag{23}$$

regularizes the strain produced by the periodic images and ensures the absolute convergence of sum (22).

The self-strain correction energy equals

$$E_{strain}^{corr} = -\frac{1}{2}P_{ij}\left(-\bar{\epsilon}_{ij}^{D}\right) = \frac{1}{2V_{cell}}\int_{V_{cell}} P_{ij}\epsilon_{ij}^{D}(\mathbf{r})d^3r. \tag{24}$$

As we only need to account for the linear elastic part of the strain field of the defect, we use the far-field approximation again, namely

$$E_{strain}^{corr} = -\frac{1}{2V_{cell}}\int_{V_{cell}} P_{ij}P_{kl}\frac{\partial}{\partial x_j}\frac{\partial}{\partial x_l}G_{ik}(\mathbf{r})d^3r. \tag{25}$$

This term corrects the total energy for the effect of elastic strain produced by the defect in the original cell. Eq. (25) has the form similar to Eq. (23), and corresponds to the first, $n = 0$, term in the series.

In practice, Eqs. (23) and (25) can be expressed and computed as surface integrals over the surface of the simulation cell. This is a simple corollary of the divergence theorem [9,21,22], namely

$$\int_{V_{cell}} P_{kl}\frac{\partial}{\partial x_j}\frac{\partial}{\partial x_l}G_{ik}(\mathbf{r})d^3r = \oint_{S_{cell}} P_{k\alpha}\frac{\partial}{\partial x_j}G_{ik}(\mathbf{r})n_\alpha dS. \tag{26}$$

Here $\mathbf{n}$ is the unit vector of external surface normal vector, and index α refers a Cartesian component of this vector. Calculating the first derivative of elastic Green's function is numerically more expedient than the second derivative, and the same applies to the calculation of surface integrals as opposed to volume integrals. Elastic Green's function as well as its first and second derivatives can be evaluated numerically using Barnett's approach [23].

A limitation of the current theory is that it only applies to a defect that is sufficiently well localized within the cell, and where its non-linear core part is some distance away from the surface of the simulation cell. This enables representing the elastic field of the defect in the neighbouring cells using the elastic dipole formalism where the defect is effectively treated as a point object. Our method does not apply to extended defects, such as dislocations, unless the dimensionality of the problem enables reducing it to a purely two-dimensional case, where dislocations are treated as infinite straight lines and where the strain field generated by every segment of a dislocation line is described by Mura's formula [24]. In this case the elastic correction energy can be computed using the method developed by Cai et al. [25].

3. Algorithm

It is not practically feasible to compute E_{DD}^{total} and E_{DD}^{corr} by summing up an infinite number of terms in the series. Provided that we include the same number of terms in both series, the sum of them, E_{DD}, converges in the limit where the cutoff distance is sufficiently large [8]. Calculating E_{DD}^{total} is relatively straightforward, since we can evaluate the second derivative of elastic Green's function numerically. The calculation of E_{DD}^{corr} is somewhat more involved as it requires evaluating integrals over the surface of the simulation cell, see Eq. (26).

A simulation cell involving PBCs usually has six faces and in general the surface integration is performed over the surface of a rhombohedron. For an arbitrary function F, the surface integral over the surface of a rhomboid in a three dimensional system of coordinates can be written as

$$\int_S F(\mathbf{r}(u,v))dS = \int_{-1}^{1}\int_{-1}^{1} F(\mathbf{r}(u,v))J(u,v)dudv \tag{27}$$

where

$$J(u,v) = \left\| \frac{\partial \mathbf{r}}{\partial u} \times \frac{\partial \mathbf{r}}{\partial v} \right\| \tag{28}$$

is the transformation Jacobian. The position vector $\mathbf{r}$ is a function of u and v in terms of the translation vectors of the simulation cell. For example, the position vector at the top and bottom surfaces of a box is

$$\mathbf{r} = \frac{u}{2}\mathbf{L}_x + \frac{v}{2}\mathbf{L}_y \pm \frac{1}{2}\mathbf{L}_z, \tag{29}$$

where the $+$ and $-$ signs in the last term correspond to the top and bottom surfaces, respectively. The Jacobian for both the top and bottom surfaces is now

$$J(u,v) = \frac{1}{4}\left\|\mathbf{L}_x \times \mathbf{L}_y\right\|. \tag{30}$$

The Jacobian for the other four surfaces can be evaluated in a similar way.

Integration from -1 to 1 is performed numerically using the nine-point Gaussian quadrature method. In the two-dimensional case, the double integration is performed in a nested manner, namely

$$\int_{-1}^{1}\int_{-1}^{1} f(u,v)dudv \approx \sum_i \sum_j w_i w_j f(u_i, v_j) \tag{31}$$

where w_i and w_j are the weights with respect to u_i and v_j. This fully defines the numerical procedure required for evaluating the surface integral in Eq. (26). A test involving eleven-point Gaussian quadrature integration was also performed, and produced the same result up to four decimal places [8].

We have verified our calculations of E_{DD} by performing summation over cubic, spherical and ellipsoidal volumes [8], gradually increasing the cut-off distance, and found that the results

were absolutely convergent. Considering the balance between efficiency and accuracy, we chose spherical summation volumes with the cutoff radius of $10 + \delta$ times translation vectors, where the magnitude of δ is small. The values computed using our code were verified numerically against the values computed numerically using the ANETO code [6], which is a FORTRAN program developed independently by Varvenne et al. for a similar purpose. The authors of Ref. [6] attribute their methodology to Cai et al. [25], who developed it for correcting the elastic interactions between dislocations in two dimensions, using an electrostatic analogy. No electrostatic analogy was used in the derivation of equations given in the preceding section of this paper.

4. Compilation of the program

CALANIE is a code written in C++. It can be compiled using any modern C++ compiler, including Intel and GNU compilers. No linking to external libraries is required. The code can be compiled in two different ways, for two different purposes. The first one is for general type *ab initio* calculations. Using g++, one can compile CALANIE using the following command line

```
$ g++ -DABINITIO -DSTRESSeV -o calanie CALANIE_2.0.cpp
```

or

```
$ g++ -DABINITIO -DSTRESSGPa -o calanie CALANIE_2.0.cpp
```

Option -DABINITIO defines the word ABINITIO in the code, such that the program is compiled for the purpose of correcting the elastic energy and obtaining the dipole tensor from the output of a general purpose *ab initio* program. Option -DSTRESSeV means that stresses in the input file should be given in eV units. In other words, the input stresses are not the macro-stresses themselves, but the macro-stresses multiplied by the cell volume. If one uses VASP [26–29], the corresponding values are given in the line entitled "Total" in the corresponding "OUTCAR" file. On the other hand, one can use a more general option -DSTRESSGPa. The stresses in the input file should then be given as the residual stresses, and should be expressed in GPa units. The sign of stresses follows the convention adopted in VASP. A value of positive stress means that the simulation cell attempts to expand, whereas a negative value of stress implies contraction.

The second compilation option is needed for analysing the relative elastic effect, assuming that a linear defect can rotate. It can be compiled using the command

```
$ g++ -DORIENTATION -o calanie CALANIE_2.0.cpp
```

This compilation command is required for analysing changes in the elastic correction energy of a defect, assuming that it can rotate freely according to Eq. (16). This enables assessing the stability of a defect under the influence of stresses developing in the supercell under PBCs. An application of this compilation option was illustrated in our earlier study [8].

5. Input and output

CALANIE uses two input files. They are *input_data* and *input_elastic*. These files need to be located in the same directory in order to execute CALANIE. Both are ASCII files.

When we use option -DABINITIO, in the *input_data* file we need to specify the translation vectors, the linear scaling factor, and the residual stresses in the perfect cell and in the cell containing a defect. They should be specified using the following format

```
box_ref_11 ???
box_ref_12 ???
box_ref_13 ???
box_ref_21 ???
box_ref_22 ???
box_ref_23 ???
box_ref_31 ???
box_ref_32 ???
box_ref_33 ???
a_lattice_ref ???

box_def_11 ???
⋮
box_def_33 ???
a_lattice_def ???

stress11_ref ???
⋮
stress33_ref ???

stress11_def ???
⋮
stress33_def ???
```

The numerical value that follows a keyword is the input value, the position of which is indicated by ??? above. Keywords **box_ref_$\alpha\beta$** and **box_def_$\alpha\beta$** are the translation vectors of the perfect reference cell and the cell containing a defect, and $\alpha, \beta = 1, 2, 3$. Keywords **a_lattice_ref** and **a_lattice_def** are linear scaling factors. Keywords **stress$\alpha\beta$_ref** and **stress$\alpha\beta$_def** are the residual stresses in the reference cell and in a cell containing a defect. One and only one value should be specified. All the nine matrix elements for the translation vectors and residual stresses are required.

If we consider a relaxed defect configuration in a simulation cell, there are two commonly used simulation conditions. One is a fixed boundary (net zero strain) condition, and the other is a net zero stress condition. In the case of a fixed boundary (net zero strain) condition, values of **box_ref_$\alpha\beta$** and **box_def_$\alpha\beta$** are the same. Values of **stress$\alpha\beta$_ref** should all be zeros, and **stress$\alpha\beta$_def** are the corresponding stress values characterizing the stress in the cell containing a defect. In the case of a stress-free condition, values of **box_def_$\alpha\beta$** are the cell translation vectors for the cell relaxed to the zero value of macrostress, whereas the values of **stress$\alpha\beta$_ref** and **stress$\alpha\beta$_def** should all vanish.

In the *input_elastic* file, the first two lines are the comment lines. The third to eighth lines contain values of elastic constants in the Voigt notation C_{ij}, in GPa units, followed by the compliance constants S_{ij}, also in the Voigt notation, given in GPa^{-1} units. The input should appear as follows

#comments

#comments

C_{11} C_{12} C_{13} C_{14} C_{15} C_{16}

C_{21} C_{22} C_{23} C_{24} C_{25} C_{26}

C_{31} C_{32} C_{33} C_{34} C_{35} C_{36}

C_{41} C_{42} C_{43} C_{44} C_{45} C_{46}

C_{51} C_{52} C_{53} C_{54} C_{55} C_{56}

C_{61} C_{62} C_{63} C_{64} C_{65} C_{66}

S_{11} S_{12} S_{13} S_{14} S_{15} S_{16}

S_{21} S_{22} S_{23} S_{24} S_{25} S_{26}

S_{31} S_{32} S_{33} S_{34} S_{35} S_{36}

S_{41} S_{42} S_{43} S_{44} S_{45} S_{46}

S_{51} S_{52} S_{53} S_{54} S_{55} S_{56}

S_{61} S_{62} S_{63} S_{64} S_{65} S_{66}

Once both input files *input_data* and *input_elastic* are available, the program can be run from the same directory by executing the command

$ ./calanie

We provide a simple python script *make_input_elastic.py* to help generate *input_elastic*. The user needs to provide a file with the name *input_elastic_Cij* with only the first eight lines of *input_elastic*. By running *make_input_elastic.py*, one generates a file *input_elastic* with the required values of S_{ij}. Sample files with names *input_data_2*, *input_elastic* and *input_elastic_Cij* are included in the distribution of CALANIE.

When using option -DORIENTATION, in *input_data* we only need to specify the translation vectors and linear scaling factor for the reference cell. We also need the values of $\Omega^{(1)}$ and $\Omega^{(2)}$ through the keywords of **Omega1** and **Omega2** in Å^3 units. A sample file named *input_data_1* illustrates this part of input. The *input_elastic* file is the same as in the previous case. However, when we run the program, we need to specify the orientation of a defect in terms of θ and ϕ, namely

$./calanie θ ϕ

The dipole tensor of the defect can be calculated using Eq. (16), followed by the calculation of its elastic correction energy.

There is no specific output file format associated with either option. Outputs are printed out directly. Values of P_{ij}, E^{app}, E^{total}_{DD}, E^{corr}_{DD}, E_{DD}, E^{corr}_{strain}, and E^{corr}_{el} are computed and displayed. The relaxation volume tensor Ω_{ij} and relaxation volume Ω_{rel} are also evaluated according to equations $\Omega_{ij} = S_{ijkl}P_{kl}$ and $\Omega_{rel} = \mathrm{Tr}(\Omega_{ij})$.

6. Applications

6.1. Ab initio calculations: Point defects in FCC gold

Elastic correction can be readily applied in the context of a calculation of formation and migration energies of point defects. We have applied CALANIE to improve the quality of *ab initio* defect energies in FCC gold, which were partially described in a study by Hofmann et al. [30]. The calculations were performed for a vacancy and several self-interstitial atom (SIA) defects, where the latter included a ⟨100⟩ dumbbell, an octahedral site interstitial, a ⟨110⟩ crowdion, and a ⟨110⟩ dumbbell.

All the *ab initio* density functional theory (DFT) calculations were performed using Vienna Ab initio Simulation Package (VASP) [26–29]. We used the revised-TPSS exchange–correlation functional [31,32]. The spin–orbit coupling was also included, to account for the band splitting and shape modification of the 5*d* bands [33–35]. The plane wave energy cut-off was 450 eV for the 11 valence electrons included in the calculation. Different sizes of simulation cells were used for different defects. The corresponding box sizes and k-point meshes are given in Table 1. All the simulation boxes were relaxed to the stress-free condition, with residual forces lower than 0.01 eV/Å. Formation energies were calculated using Eq. (18) with respect to a perfect crystal, using a similar cell size and the same k-point mesh.

Elastic constants are also required for calculating E^{app} and E^{corr}_{el}. They were calculated using the Le Page and Saxe method [36], using a 4-atom cubic cell. From *ab initio* calculations, we obtained $C_{11} = 210.55$ GPa, $C_{12} = 168.11$ GPa and $C_{44} = 49.96$ GPa. These values are compatible with the low temperature experimental values, which are $C_{11} = 201.63$ GPa, $C_{12} = 169.67$ GPa and $C_{44} = 45.44$ GPa [37]. The calculated lattice constant is 4.075 Å, whereas the experimental value is 4.07833 Å [38].

Table 1
The number of atoms, approximate cell size (in the units of cubic unit cell size), and the k-point mesh that were used in the calculations of vacancy, ⟨100⟩ dumbbell, octahedral site interstitial, ⟨110⟩ crowdion, and ⟨110⟩ dumbbell defects in FCC gold.

	No. of atoms	Approx. cell size	k-points
Vac	107	3 × 3 × 3	4 × 4 × 4
⟨100⟩d	145	3 × 3 × 4	4 × 4 × 3
Octa	109	3 × 3 × 3	4 × 4 × 4
⟨110⟩c	193	3 × 4 × 4	4 × 3 × 3
⟨110⟩d	193	3 × 4 × 4	4 × 3 × 3

Table 2
The total energy E_{def} of a simulation box containing a defect, the total energy E_{perf} of a perfect lattice simulation cell, the applied strain energy E^{app}, the elastic correction energy E^{corr}_{el}, and the formation energy E^{F}_{def} of a vacancy, a ⟨100⟩ dumbbell, an octahedral site interstitial, a ⟨110⟩ crowdion, and a ⟨110⟩ dumbbell in FCC gold. The value of E^{F}_{def} with no elastic correction, corresponding to $E^{app} = 0$ and $E^{corr}_{el} = 0$, is also given for comparison. All the values are given in eV units.

	E_{def}	E_{perf}	E^{app}	E^{corr}_{el}	E^{F}_{def}	E^{F}_{def} (no corr)
Vac	4056.141572	4093.103600	−0.010717	0.00848	0.939	0.937
⟨100⟩d	5499.210885	5457.464770	−0.273714	0.18303	3.938	3.847
Octa	4135.011821	4093.103600	−0.375941	0.28347	4.102	4.009
⟨110⟩c	7318.341711	7276.601601	−0.275946	0.15802	3.959	3.841
⟨110⟩d	7318.342569	7276.601601	−0.275557	0.15747	3.960	3.842

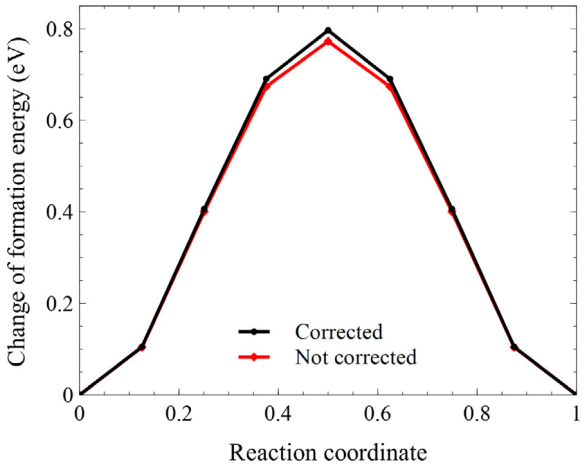

Fig. 1. Variation of the formation energy of a vacancy during its transition from an equilibrium position to a nearest neighbour equilibrium position. A small difference can be observed between the cases studied with and without applying the elastic correction.

Table 3
Elastic dipole tensor P_{ij}, in eV units, computed for a vacancy, a ⟨100⟩ dumbbell, an octahedral site interstitial, an ⟨110⟩ crowdion, and a ⟨110⟩ dumbbell in FCC gold.

	P_{11}	P_{22}	P_{33}	P_{12}	P_{23}	P_{31}
Vac	−6.760	−6.760	−6.760	0.000	0.000	0.000
⟨100⟩d	36.667	39.612	39.612	0.000	0.000	0.000
Octa	39.529	39.529	39.529	0.000	0.000	0.000
⟨110⟩c	38.856	38.856	41.084	11.199	0.000	0.000
⟨110⟩d	38.742	38.742	41.332	11.155	0.000	0.000

Table 4
Relaxation volume tensor Ω_{ij} and relaxation volume Ω_{rel}, in atomic volume units, computed for a vacancy, a ⟨100⟩ dumbbell, an octahedral site interstitial, a ⟨110⟩ crowdion, and a ⟨110⟩ dumbbell in FCC gold.

	Ω_{11}	Ω_{22}	Ω_{33}	Ω_{12}	Ω_{23}	Ω_{31}	Ω_{rel}
Vac	−0.117	−0.117	−0.117	0.000	0.000	0.000	−0.351
⟨100⟩d	0.231	0.888	0.888	0.000	0.000	0.000	2.008
Octa	0.685	0.685	0.685	0.000	0.000	0.000	2.068
⟨110⟩c	0.520	0.520	1.018	1.062	0.000	0.000	2.058
⟨110⟩d	0.494	0.494	1.072	1.057	0.000	0.000	2.059

The corrected defect formation energies E^F_{def}, applied strain energies E^{app}, elastic correction energies E^{corr}_{el}, and the formation energy of defects with no correction applied, that is ignoring E^{app} and E^{corr}_{el}, are given in Table 2. The data given in the Table show that a ⟨100⟩ dumbbell has the lowest formation energy, whereas a ⟨110⟩ crowdion has the lowest formation energy if the elastic correction is not included. However, we should note that the energy difference between a ⟨100⟩ dumbbell, a ⟨110⟩ crowdion and a ⟨110⟩ dumbbell is very small. Since the accuracy of a DFT calculation is in the meV range, it is hard to draw a definitive conclusion about the structure of the most stable SIA defect configuration in gold.

Elements of elastic dipole tensors P_{ij}, in eV units, are given in Table 3, whereas the elements of the relaxation volume tensor Ω_{ij} and the total relaxation volume Ω_{rel}, in atomic volume units, are given in Table 4. We note that their values are correlated with the symmetry of a particular defect. Indeed, the calculated values of P_{ij} and Ω_{ij} might be more significant than the calculated values of the elastic correction terms. One can readily use them to evaluate the strength of defect–defect interactions through linear elasticity theory [5–9], and even apply it to examine the stress profile of an irradiated component on a macroscopic scale, if the distribution of defects is computed starting from a neutron transport calculation [17].

Elastic correction can also be applied to non-equilibrium configurations. For example, it can be applied to the atomic configurations describing the migration pathway of a defect. We performed a nudged elastic band calculation [39,40] of vacancy migration in gold, where seven NEB images were used. A vacancy hops from an equilibrium position to the nearest neighbour equilibrium position in the y–z plane. Fig. 1 shows the change in the formation energy with and without the elastic energy correction. The computed migration energy agrees well with the experimental value of 0.71 ± 0.05 eV [38]. The effect of applying the elastic correction is not prominent in this case, as the stress field induced in the lattice by a vacancy is relatively weak.

On the other hand, we observe a change in P_{ij} during the transition, illustrated in Fig. 2, which can give rise to effects of

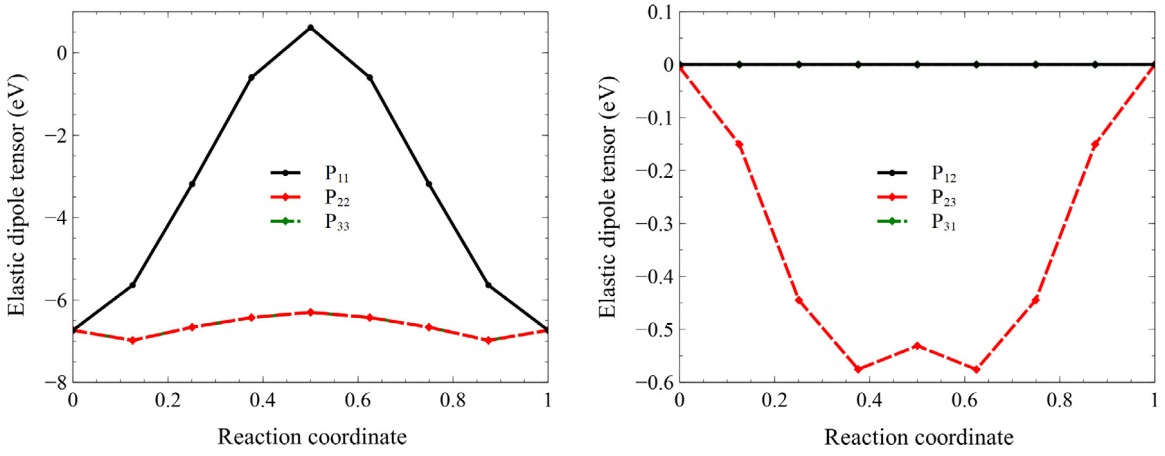

Fig. 2. Elastic dipole tensor of a vacancy moving along a migration pathway in the y–z plane. Owing to the symmetry of the defect, $P_{22} = P_{33}$ and $P_{12} = P_{31} = 0$.

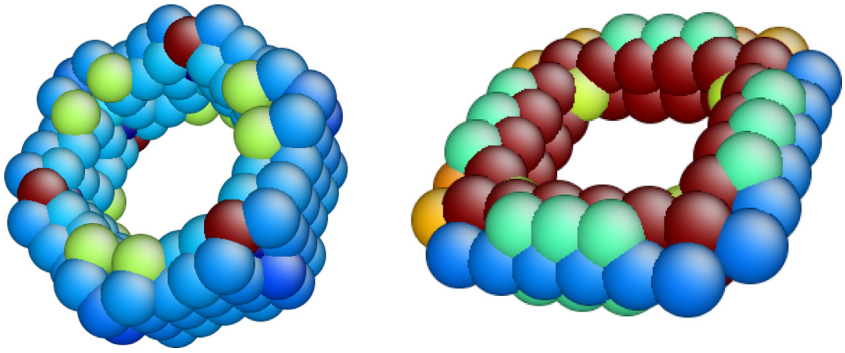

Fig. 3. Atomic configuration of (left) a circular $\frac{1}{2}\langle 111\rangle$ and (right) a square ⟨100⟩ self-interstitial atom loop. Both loops contain 61 self-interstitial atoms. Bulk atoms were filtered out according to the central symmetry parameter criterion.

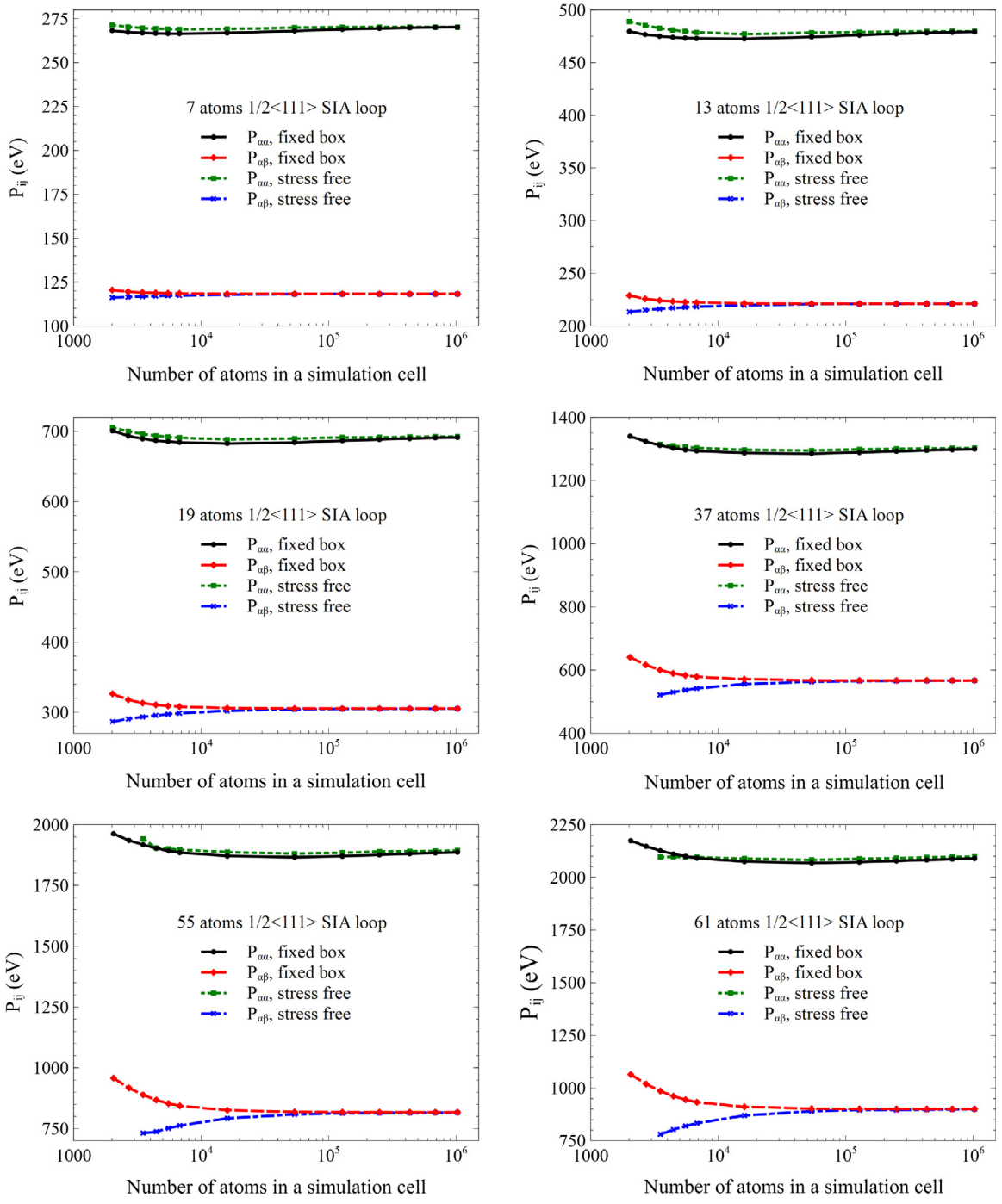

Fig. 4. Elastic dipole tensors of $\frac{1}{2}\langle 111\rangle$ self-interstitial atom loops containing 7, 13, 19, 37, 55, and 61 atoms as functions of the simulation cell size. $P_{\alpha\alpha}$ are the diagonal terms, whereas $P_{\alpha\beta}$ are the off-diagonal terms. Elements of the elastic dipole tensor are computed using the condition that the simulation cell shape was fixed to match the perfect lattice case, or allowed to relax to a stress-free condition.

anisotropic diffusion under applied external stress, or the stress induced by other defects, for example dislocations [22]. The anisotropic diffusion tensor in the linear approximation in the spatially slow varying external strain field $\epsilon_{ij}(\mathbf{R})$ can be written following the analysis by Dederichs and Schroeder [41] as

$$D_{ij}(\mathbf{R}) = \frac{1}{2}\sum_h \lambda_h r_i^h r_j^h \exp\left(\frac{\epsilon_{kl}(\mathbf{R})(P_{kl}^{sd,h} - P_{kl}^{eq})}{k_B T}\right), \tag{32}$$

where summation is performed over all the possible hopping sites h, $\lambda_h = \nu_0 \exp(-E_D^{M,h}/k_B T)$ is the atomic jump frequency, ν_0 is the attempt frequency, $E_D^{M,h}$ is the migration barrier in the corresponding hopping direction, r_i^h is a Cartesian component of the hopping direction vector, $P_{kl}^{sd,h}$ and P_{kl}^{eq} are the elastic dipole tensors at the saddle point and at an equilibrium position. The value of D_{ij} for a given value of strain can be evaluated using the data given here. Anisotropic diffusion of point defects under applied stress induced by a screw dislocation has been explored by Sivak and Sivak [42] in fcc copper using kinetic Monte Carlo simulations.

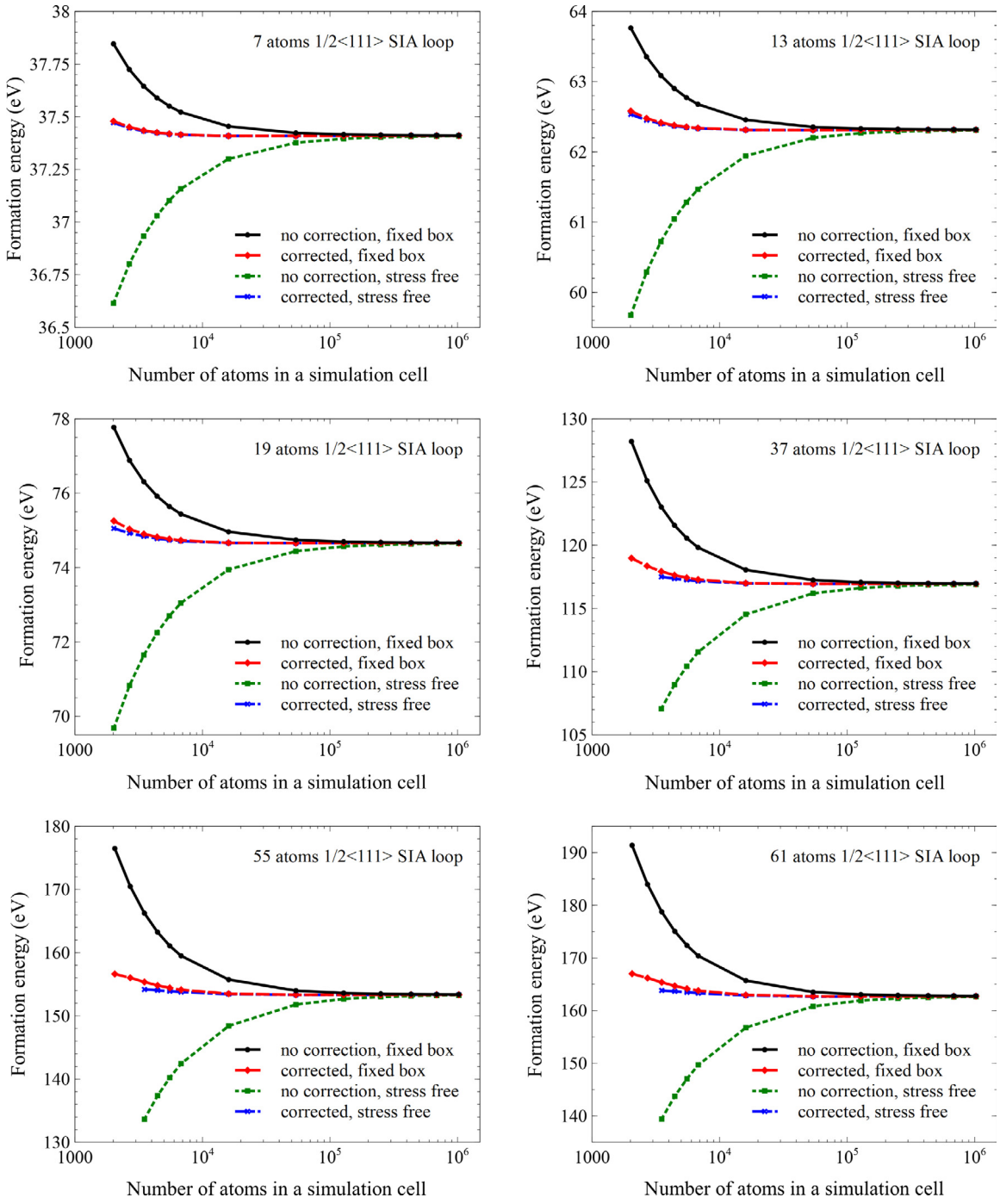

Fig. 5. Formation energy E^F_{def} of $\frac{1}{2}\langle 111\rangle$ self-interstitial atom loops containing 7, 13, 19, 37, 55, and 61 atoms shown as a function of the simulation cell size. The E^F_{def} is calculated with elastic correction applied, i.e. using Eq. (18), or without the correction, i.e. ignoring the E^{app} and E^{corr}_{el}. Both are calculated under the condition that the simulation cell shape was fixed to match the perfect lattice case, or was allowed to relax to a stress-free condition.

6.2. Molecular statics: Dislocation loop in tungsten

Elastic field of a mesoscopic defect is much stronger than that of a point defect. Elastic correction is also larger for a defect of larger size in a small simulation box. For example, an *ab initio* calculation is usually limited to a few hundred atoms. The formalism developed in this paper can be applied to any localized defect irrespective to its structure. If the elastic dipole tensor P_{ij} of the defect is known, one can use it to compute the corrected defect formation energy E^F_{def} using Eq. (18), provided that the strain field at the surface of a simulation box is well approximated by linear elasticity. We would like to examine the convergence of the P_{ij} and E^F_{def} of mesoscopic scale defects as a function of simulation cell size and simulation conditions.

We have investigated this issue using molecular statics. Molecular static allows us to do highly accurate calculations using very large simulation cells within a reasonable amount of computation time. We used the Mason–Nguyen–Manh–Becquart (MNB) [43] potential for tungsten. The calculated elastic constants for this potential are $C_{11} = 526.83$ GPa, $C_{12} = 205.28$ GPa, and $C_{44} = 160.63$ GPa. All the calculations were performed using LAMMPS [44]. Atomic relaxations were performed using the conjugate gradient method. We have investigated circular $\frac{1}{2}\langle 111\rangle$ self-interstitial atom (SIA) loops containing 7, 13, 19, 37, 55 and 61

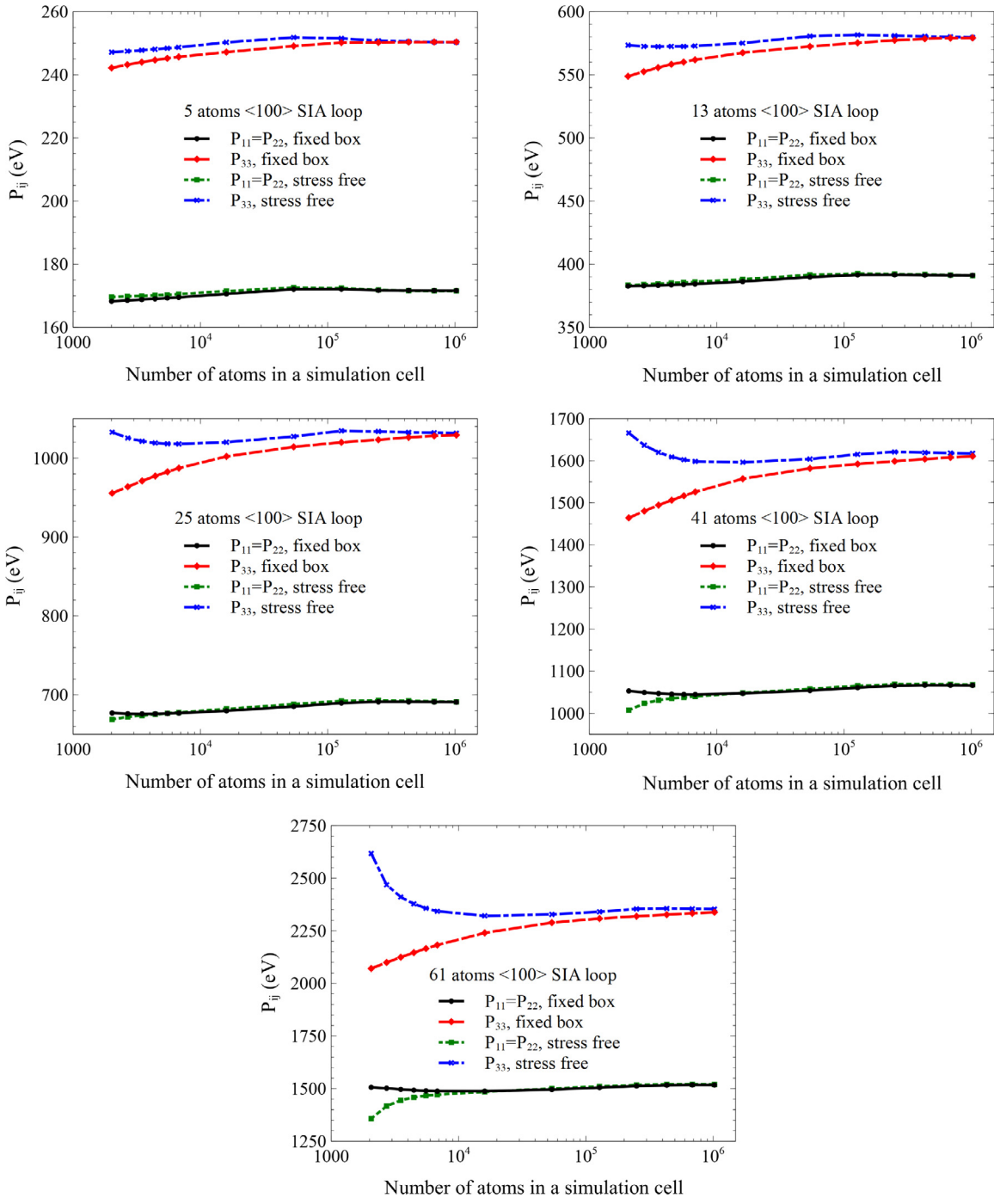

Fig. 6. Elements of elastic dipole tensors of ⟨100⟩ self-interstitial atom loops containing 5, 13, 25, 41, and 61 atoms plotted as a function of the simulation cell size. The off-diagonal terms of the dipole tensor vanish because of symmetry. The elastic dipole tensor is calculated under the condition that the simulation box shape was fixed to match the perfect lattice case, or was allowed to relax to a stress-free condition.

atoms, and square ⟨100⟩ SIA loops containing 5, 13, 25, 41 and 61 atoms, using simulation cells of varying size involving from 2000 to 1 million atoms. Two sets of calculations were performed. In one set, the shape and volume of the simulation cell remained fixed as the same as in the perfect lattice case. In the other set, the cell was allowed to relax to a stress-free condition. The loop structure of a circular $\frac{1}{2}\langle 111\rangle$ and square ⟨100⟩ loop with 61 atoms are shown in Fig. 3. They were generated using AtomEye software [45], where bulk atoms were filtered using the central symmetry parameter criterion.

Fig. 4 shows elements of the elastic dipole tensor of $\frac{1}{2}\langle 111\rangle$ SIA loops plotted as functions of the simulation cell size. Due to the symmetry of the defect, values of diagonal terms are all the same and labelled $P_{\alpha\alpha}$, whereas the off-diagonal terms also have the same values and are labelled $P_{\alpha\beta}$. We see that both the fixed cell and stress-free condition calculations converge to the same value if the simulation box is large enough. Under the stress-free condition, when the simulation cell size is in the range of $10 \times 10 \times 10$ and $11 \times 11 \times 11$ unit cells, the cells containing 55 and 61 atoms loops deform significantly. The calculated values of P_{ij} do not reflect the correct symmetry of a $\frac{1}{2}\langle 111\rangle$ SIA loop type, so we have discarded these data.

Fig. 5 shows the corrected formation energy calculated using the data shown in Fig. 4. We note that the elastic correction

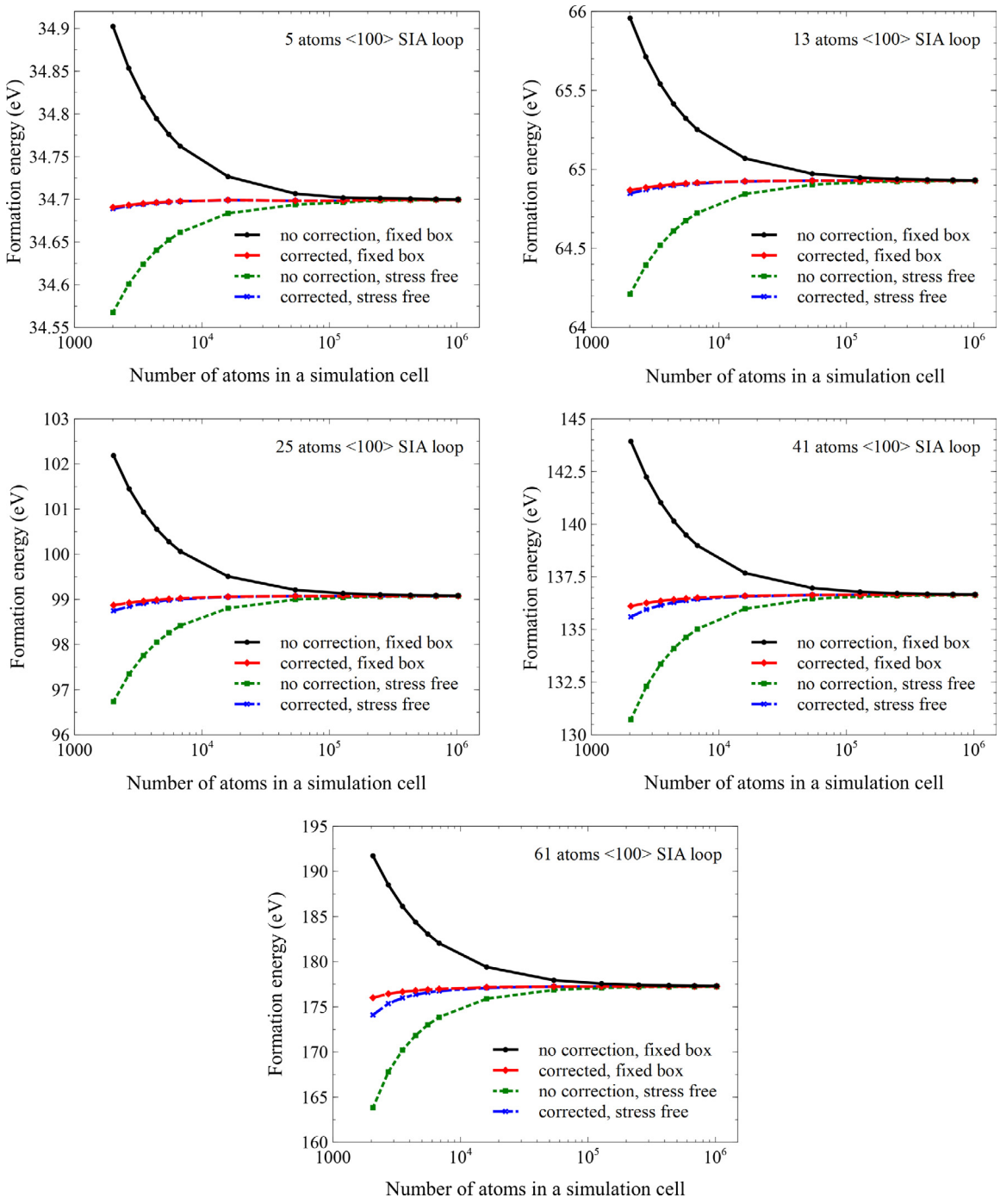

Fig. 7. Formation energy E^F_{def} of ⟨100⟩ self-interstitial atom loops containing 5, 13, 25, 41, and 61 atoms shown as a function of the simulation cell size. Values of E^F_{def} were calculated with elastic correction applied, i.e. using Eq. (18), or with no correction, i.e. ignoring E^{app} and E^{corr}_{el}. Both were calculated under the condition that the simulation box shape was fixed to match the perfect lattice case, or was allowed to relax to a stress-free condition.

converges well in the limit of large simulation box. At the same time, we see that although the fixed cell and stress-free condition calculations suggest different values prior to the application of elastic correction, their values become comparable when this correction is applied. For mesoscopic scale loops, e.g. a 61 atom loop, the difference can be fairly large if the correction is not applied.

Figs. 6 and 7 show the elements of the dipole tensor and formation energy of ⟨100⟩ loops as functions of the cell size. Due to the symmetry, we know that the elements of dipole tensor $P_{11} = P_{22}$, $P_{33} \neq 0$, and that the off-diagonal elements all vanish. We observe a similar pattern for the ⟨100⟩ loops as for the $\frac{1}{2}\langle 111\rangle$ loops. The error in P_{ij} becomes larger when the size of the defect becomes comparable to the size of the simulation box. This is a consequence of the fact that the derivation of the dipole tensor formalism is based on the linear elasticity approximation.

When the size of the simulation cell is small, the deformation of the lattice near the surface of the cell due to a defect may become very large and hence non-linear. This makes the values of P_{ij} computed in the linear elasticity approximation inaccurate. Nevertheless, it still helps correct the formation energy for various simulation cell conditions, such as in the two limiting cases of

the fixed box and stress-free conditions. This even enables calculating the formation energy of a relatively large size defect using a relatively small simulation cell with higher confidence, which is important especially in the context of an *ab initio* calculation where the cost of computation is high.

7. Conclusion

In this study, we presented a summary of the fundamental theory, algorithms and numerical implementation of computer program CALANIE, intended for the evaluation of anisotropic elastic interaction energy correction associated with the use of periodic boundary conditions (PBCs). The theory is based on the linear elasticity approximation. The elastic interaction of a defect with its periodic images is approximated and evaluated using the elastic dipole and elastic Green's function formalism. The elements of the elastic dipole tensor of a defect can be computed in same electronic or atomic scale simulation as the formation energy of the defect. Elastic Green's function and its first and second derivatives can also be calculated numerically if the elastic constants of the material are known. Working examples together with the relevant input files are provided. Compilation of CALANIE can be performed using any modern C++ compiler.

Applications of the program are illustrated using two case studies as examples. One example involves *ab initio* calculations of point defects in FCC gold. We show that elastic correction can be applied not only to equilibrium, but also to non-equilibrium configurations, for example to the treatment of diffusion of vacancies in applied external elastic field. Other applications involve relatively large, mesoscopic scale defects. We investigate the convergence of calculations of elements of dipole tensors and formation energies in the large simulation cell limit. We show that the treatment of elastic correction can improve the quality of evaluation of the formation energy even in the limit where the size of the defect is comparable with the size of the simulation cell.

Declaration of competing interest

The authors declare that they have no known competing financial interests or personal relationships that could have appeared to influence the work reported in this paper.

Acknowledgements

This work has been carried out within the framework of the EUROFusion Consortium and has received funding from the Euratom research and training programmes 2014–2018 and 2019–2020 under grant agreement No. 633053 and from the RCUK Energy Programme [grant No. EP/T012250/1]. To obtain further information on the data and models underlying the paper please contact PublicationsManager@ukaea.uk. The views and opinions expressed herein do not necessarily reflect those of the European Commission.

References

[1] W. Cai, W.D. Nix, Imperfections in Crystalline Solids, Cambridge University Press, Cambridge, England, UK, 2016.
[2] A.E. Sand, K. Nordlund, S.L. Dudarev, J. Nucl. Mater. 455 (1) (2014) 207–211, Proceedings of the 16th International Conference on Fusion Reactor Materials, ICFRM-16. http://dx.doi.org/10.1016/j.jnucmat.2014.06.007.
[3] A.E. Sand, M.J. Aliaga, M.J. Caturla, K. Nordlund, Europhys. Lett. 115 (3) (2016) 36001, http://dx.doi.org/10.1209/0295-5075/115/36001.
[4] J. Byggmästar, F. Granberg, A.E. Sand, A. Pirttikoski, R. Alexander, M.-C. Marinica, K. Nordlund, J. Phys.: Condens. Matter 31 (24) (2019) 245402, http://dx.doi.org/10.1088/1361-648X/ab0682.
[5] S.L. Dudarev, M.R. Gilbert, K. Arakawa, H. Mori, Z. Yao, M.L. Jenkins, P.M. Derlet, Phys. Rev. B 81 (2010) 224107, http://dx.doi.org/10.1103/PhysRevB.81.224107.
[6] C. Varvenne, F. Bruneval, M.-C. Marinica, E. Clouet, Phys. Rev. B 88 (2013) 134102, http://dx.doi.org/10.1103/PhysRevB.88.134102.
[7] C. Varvenne, E. Clouet, Phys. Rev. B 96 (2017) 224103, http://dx.doi.org/10.1103/PhysRevB.96.224103.
[8] S.L. Dudarev, P.-W. Ma, Phys. Rev. Mater. 2 (2018) 033602, http://dx.doi.org/10.1103/PhysRevMaterials.2.033602.
[9] P.-W. Ma, S.L. Dudarev, Phys. Rev. Mater. 3 (2019) 013605, http://dx.doi.org/10.1103/PhysRevMaterials.3.013605.
[10] M. Durrand-Charre, Microstructure of Steels and Cast Irons, Springer-Verlag, Berlin, 2003.
[11] W. Kohn, L.J. Sham, Phys. Rev. 140 (1965) A1133–A1138, http://dx.doi.org/10.1103/PhysRev.140.A1133.
[12] P. Hohenberg, W. Kohn, Phys. Rev. 136 (1964) B864–B871, http://dx.doi.org/10.1103/PhysRev.136.B864.
[13] D.R. Mason, X. Yi, M.A. Kirk, S.L. Dudarev, J. Phys.: Condens. Matter 26 (37) (2014) 375701, http://dx.doi.org/10.1088/0953-8984/26/37/375701.
[14] G. Subramanian, D. Perez, B.P. Uberuaga, C.N. Tomé, A.F. Voter, Phys. Rev. B 87 (2013) 144107, http://dx.doi.org/10.1103/PhysRevB.87.144107.
[15] E. Martínez, M.J. Caturla, J. Marian, in: W. Andreoni, S. Yip (Eds.), Handbook of Materials Modeling: Applications: Current and Emerging Materials, Springer International Publishing, Cham, 2018, pp. 1–32, http://dx.doi.org/10.1007/978-3-319-50257-1_137-1.
[16] G. Leibfried, N. Breuer, Point Defects in Metals, Springer, Berlin, 1978, p. 161.
[17] S.L. Dudarev, D.R. Mason, E. Tarleton, P.-W. Ma, A.E. Sand, Nucl. Fusion 58 (12) (2018) 126002, http://dx.doi.org/10.1088/1741-4326/aadb48.
[18] D.R. Mason, D. Nguyen-Manh, M.-C. Marinica, R. Alexander, A.E. Sand, S.L. Dudarev, J. Appl. Phys. 126 (2019) 075112, http://dx.doi.org/10.1063/1.5094852.
[19] C. Domain, C.S. Becquart, Phys. Rev. B 65 (2001) 024103, http://dx.doi.org/10.1103/PhysRevB.65.024103.
[20] E. Clouet, S. Garruchet, H. Nguyen, M. Perez, C.S. Becquart, Acta Mater. 56 (14) (2008) 3450–3460, http://dx.doi.org/10.1016/j.actamat.2008.03.024, http://www.sciencedirect.com/science/article/pii/S1359645408002218.
[21] T. Jourdan, J. Mech. Phys. Solids 125 (2019) 762–773, http://dx.doi.org/10.1016/j.jmps.2019.02.002, http://www.sciencedirect.com/science/article/pii/S0022509618309827.
[22] P.-W. Ma, S.L. Dudarev, Phys. Rev. Mater. 3 (2019) 063601, http://dx.doi.org/10.1103/PhysRevMaterials.3.063601, https://link.aps.org/doi/10.1103/PhysRevMaterials.3.063601.
[23] D.M. Barnett, Phys. Status Solidi B 49 (2) (1972) 741–748, http://dx.doi.org/10.1002/pssb.2220490238.
[24] T. Mura, Micromechanics of Defects in Solids, 2nd, Rev. Ed., Kluwer Academic Publishers, Netherlands, 1987, p. 47.
[25] W. Cai, V.V. Bulatob, J. Chang, J. Li, S. Yip, Phil. Mag. 83 (5) (2003) 539–567, http://dx.doi.org/10.1080/0141861021000051109.
[26] G. Kresse, J. Hafner, Phys. Rev. B 47 (1993) 558–561, http://dx.doi.org/10.1103/PhysRevB.47.558.
[27] G. Kresse, J. Hafner, Phys. Rev. B 49 (1994) 14251–14269, http://dx.doi.org/10.1103/PhysRevB.49.14251.
[28] G. Kresse, J. Furthmüller, Comput. Mater. Sci. 6 (1) (1996) 15–50, http://dx.doi.org/10.1016/0927-0256(96)00008-0, http://www.sciencedirect.com/science/article/pii/0927025696000080.
[29] G. Kresse, J. Furthmüller, Phys. Rev. B 54 (1996) 11169–11186, http://dx.doi.org/10.1103/PhysRevB.54.11169.
[30] F. Hofmann, E. Tarleton, R.J. Harder, N.W. Phillips, P.-W. Ma, J.N. Clark, I.K. Robinson, B. Abbey, W. Liu, C.E. Beck, Sci. Rep. 7 (2017) 45993, http://dx.doi.org/10.1038/srep45993.
[31] J.P. Perdew, A. Ruzsinszky, G.I. Csonka, L.A. Constantin, J. Sun, Phys. Rev. Lett. 103 (2009) 026403, http://dx.doi.org/10.1103/PhysRevLett.103.026403.
[32] J. Sun, M. Marsman, G.I. Csonka, A. Ruzsinszky, P. Hao, Y.-S. Kim, G. Kresse, J.P. Perdew, Phys. Rev. B 84 (2011) 035117, http://dx.doi.org/10.1103/PhysRevB.84.035117.
[33] A.D. Corso, A.M. Conte, Phys. Rev. B 71 (2005) 115106, http://dx.doi.org/10.1103/PhysRevB.71.115106.
[34] N.E. Christensen, B.O. Seraphin, Phys. Rev. B 4 (1971) 3321–3344, http://dx.doi.org/10.1103/PhysRevB.4.3321.
[35] T. Rangel, D. Kecik, P.E. Trevisanutto, G.-M. Rignanese, H. Van Swygenhoven, V. Olevano, Phys. Rev. B 86 (2012) 125125, http://dx.doi.org/10.1103/PhysRevB.86.125125.
[36] Y. Le Page, P. Saxe, Phys. Rev. B 65 (2002) 104104, http://dx.doi.org/10.1103/PhysRevB.65.104104.

[37] J.R. Neighbours, G.A. Alers, Phys. Rev. 111 (1958) 707–712, http://dx.doi.org/10.1103/PhysRev.111.707.
[38] P. Ehrhart, P. Jung, H. Schultz, H. Ullmaier, in: H. Ullmaier (Ed.), Landolt-Börnstein - Group III Condensed Matter · Volume 25: "Atomic Defects in Metals", Springer-Verlag, Berlin Heidelberg, 1991, http://dx.doi.org/10.1007/10011948_45.
[39] G. Mills, H. Jónsson, G.K. Schenter, Surf. Sci. 324 (2) (1995) 305–337, http://dx.doi.org/10.1016/0039-6028(94)00731-4, http://www.sciencedirect.com/science/article/pii/0039602894007314.
[40] H. Jónsson, G. Mills, K.W. Jacobsen, Classical and Quantum Dynamics in Condensed Phase Simulations, World Scientific, 1998, pp. 385–404, http://dx.doi.org/10.1142/9789812839664_0016.
[41] P.H. Dederichs, K. Schroeder, Phys. Rev. B 17 (1978) 2524–2536, http://dx.doi.org/10.1103/PhysRevB.17.2524.
[42] A.B. Sivak, P.A. Sivak, Crystallogr. Rep. 59 (3) (2014) 407–414, http://dx.doi.org/10.1134/S1063774514030183.
[43] D.R. Mason, D. Nguyen-Manh, C.S. Becquart, J. Phys.: Condens. Matter 29 (50) (2017) 505501, http://dx.doi.org/10.1088/1361-648x/aa9776.
[44] S. Plimpton, J. Comput. Phys. 117 (1) (1995) 1–19, http://dx.doi.org/10.1006/jcph.1995.1039.
[45] J. Li, Modelling Simulation Mater. Sci. Eng. 11 (2) (2003) 173–177, http://dx.doi.org/10.1088/0965-0393/11/2/305.